Journal of Nuclear Materials 396 (2010) 130–143

Contents lists available at ScienceDirect

Journal of Nuclear Materials

journal homepage: www.elsevier.com/locate/jnucmat

The first step for delayed hydride cracking in zirconium alloys

G.A. McRae [a,b], C.E. Coleman [b,*], B.W. Leitch [b]

[a] Department of Mechanical and Aerospace Engineering, Carleton University, Ottawa, Ontario, Canada K1S 5B6
[b] Atomic Energy of Canada Limited, Chalk River Laboratories, Chalk River, Ontario, Canada K0J 1J0

ARTICLE INFO

Keywords:
Delayed hydride cracking velocity
Zirconium
Diffusion first model
Crack incubation

ABSTRACT

Two models for delayed hydride cracking (DHC) in zirconium alloys are distinguished by their first step:

- The loading of a crack induces hydride precipitation. The hydride is postulated to create a hydrogen concentration gradient, where the bulk concentration is greater than that at the crack tip. This concentration gradient is taken as the driving force for diffusion of hydrogen to the crack tip, and subsequent hydride growth. This model is called the precipitate first model (PFM).
- The tensile stress at the crack tip induces a gradient in chemical potential that promotes the diffusion of hydrogen to the crack tip. Hydrides form if the hydrogen concentration reaches the solubility limit for hydride precipitation. The mechanism is postulated to create a hydrogen concentration gradient, where the bulk concentration is lower than that at the crack tip. The gradient in chemical potential is taken as the driving force for diffusion of hydrogen to the crack tip, and subsequent hydride growth. This model is called the diffusion first model (DFM).

The second model, DFM, is developed. This model is shown to describe the main features of the experimental observations of DHC, without invoking new phenomena, such as reduction in the solubility limit for precipitation of hydride, as required by the PFM.

1. Introduction

A time-dependent mechanism of fracture that requires cracking of zirconium hydride has been responsible for several failures of zirconium alloy components in both nuclear reactors [1–3] and chemical plants [4]. The mechanism is called delayed hydride cracking or DHC. Similar failures are observed in other hydride forming metals [5]. The mechanism requires a component or specimen to contain a stress-raiser, such as a crack, and a source of tensile stress, either residual or externally imposed.

DHC has been extensively reviewed [5–9] showing that its phenomenology includes the following observations:

(a) The microstructural feature responsible for cracking is precipitation of zirconium hydride formed at the stress-raiser. The precipitates are usually in the form of a collection of platelets, with normals parallel with the maximum tensile stress.
(b) Despite Observation (a), DHC can take place when no hydrides are present in the bulk.
(c) Time is required between the imposition of the stress and the start of cracking: the incubation time. Cracking of the hydride is rapid once a critical condition, associated with its size, is reached. Since time is required to re-establish the critical condition, subsequent cracking is intermittent. On the fracture surface of Zr–2.5Nb each cracking step is usually associated with a striation, representing broken hydrides and a small amount of ductile fracture of the zirconium matrix.
(d) A threshold condition for stressing, usually characterized as K_{IH}, has to be exceeded before cracking will start, but thereafter the crack velocity, v_c, has little or no dependence on K_I, Fig. 1.
(e) The temperature dependence of v_c is complicated, Fig. 2. The maximum value of v_c has an apparent Arrhenius behaviour described by

$$v_c = v_o \exp(-Q/RT) \quad (1)$$

where Q is the activation energy for DHC in kJ/mol, R is the Gas Constant (8.314 kJ/mol K), T is the temperature in K and v_o is a constant. If the temperature is attained by heating from T_1 in Fig. 2, initially v_c follows Eq. (1), but as the temperature is increased v_c starts to decline at T_2 and cracking eventually stops at T_3. On cooling from a high temperature, T_4, a temperature is reached where cracking will reinitiate at T_5 and reach a maximum value at T_6. This behaviour has been

* Corresponding author. Tel.: +1 613 584 2804.
E-mail addresses: gmcrae@mae.carleton.ca (G.A. McRae), colemanc@aecl.ca (C.E. Coleman), leitchb@aecl.ca (B.W. Leitch).

0022-3115/$ - see front matter Crown Copyright © 2009 Published by Elsevier B.V. All rights reserved.
doi:10.1016/j.jnucmat.2009.08.019

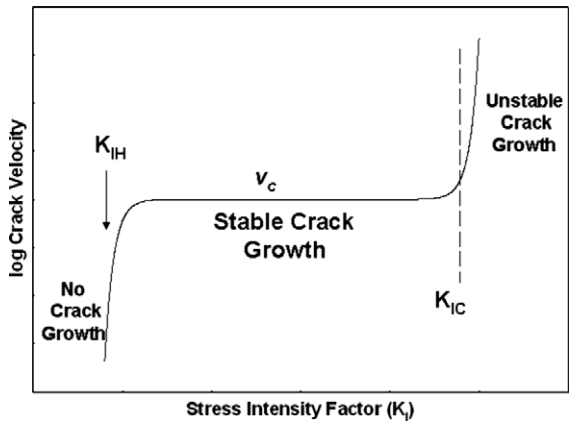

Fig. 1. The dependence of crack velocity on stress intensity factor, K_I.

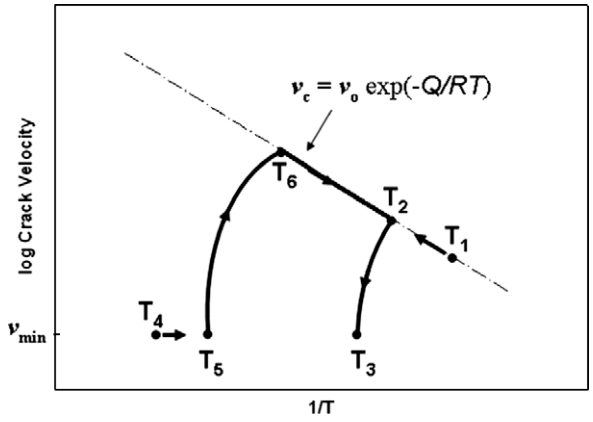

Fig. 2. Schematic diagram of the temperature dependence of DHC in zirconium alloys showing the effect of heating and cooling. v_{min} is the minimum detectable velocity.

associated with the large 'hysteresis' in the temperature dependence of the terminal solid solubility for hydrogen in zirconium when dissolving (TSSD) or precipitating (TSSP) hydrides [10–13]. Up to 1 at.% (112 parts-per-million by weight, or ppm) hydrogen, the temperature on heating, above which all the hydrides have dissolved, T_D, is about 60 °C greater than the temperature on cooling, when the hydrides start to precipitate, T_P. Fig. 3 shows two curves that depict the standard TSS lines for hydrogen in zirconium on heating, representing dissolution (TSSD), and cooling, representing precipitation (TSSP). At any temperature, the concentration of hydrogen in solution is much higher for the precipitation solvus, C_P, than for dissolution, C_D. For example, in Zr–2.5Nb at 250 °C, C_D is 29.3 ppm while C_P is 65.7 ppm [14].

DHC requires three basic steps. These steps are (1) the nucleation of a hydride at the stress-raiser followed by (2) growth of the hydride until (3) the conditions for its fracture are satisfied. Repetition of these three steps leads to crack growth. The first step has been modeled by:

Stress-induced precipitation, which implies that C_P is decreased and T_P is increased at the stress-raiser. This process will be called the precipitation first model (PFM).

Hydrogen diffusion up the hydrostatic stress gradient to the stress raiser where hydride precipitates when the increased hydrogen concentration exceeds C_P. This process will be called the diffusion first model (DFM).

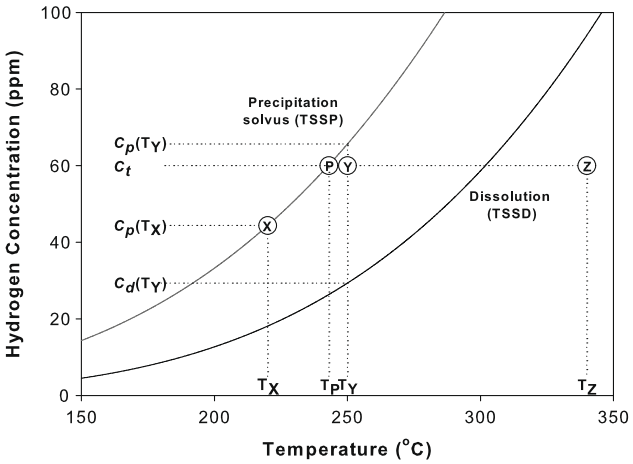

Fig. 3. The TSS lines for Zr–2.5Nb [14] and some points that are used in the text to illustrate the DFM and to distinguish it from the PFM.

The models are considered for two situations: when hydrides are present in the zirconium matrix and when all the hydrogen is in solution. These cases are illustrated schematically in Fig. 3. Consider a cracked specimen containing a total hydrogen concentration of C_t heated to temperature T_Z where all the hydrogen is in solution. After cooling to T_Y between the TSSP and TSSD lines, again no hydrides are present. On loading and applying PFM, precipitates are formed and the concentration of hydrogen in solution at the crack tip is lowered. In contrast, for cracking by DFM at T_Y the hydrogen concentration in solution increases at the crack tip up to C_P because of the stress gradient.

When the specimen is cooled to the solvus for precipitation, T_P, hydrides can form in the zirconium matrix. On further cooling to T_X, the hydrogen concentration in solution everywhere in the matrix is reduced as hydrides precipitate. On loading and applying PFM, hydrides are instantaneously formed at the crack tip reducing the hydrogen concentration in solution at the crack tip relative to the bulk. With DFM there is likewise no initial concentration gradient, however, hydrogen in solution moves to the crack tip under the influence of the stress gradient and, upon reaching the threshold for nucleation, hydrides form.

Simpson and Ells [15] suggested both the PFM and the DFM in their explanation of cracking at a weld in Zr–2.5Nb. In a fuller model, Dutton and Puls and their co-workers [16–19] also invoked both the PFM and the DFM at T_X, Fig. 3. Here the situation modelled was the development of a hydride in a region of size ℓ adjacent to the crack tip and an array of hydrides a distance L from a crack tip (representing the interhydride spacing). In the PFM, because of the volume increase during hydride precipitation, the tensile forces from the imposed stress are able to do work and enhance the precipitation step. Because of the perceived effect of hydrostatic stress on the local terminal solubility of hydrogen in zirconium, the concentration of hydrogen in solution at L is greater than the concentration at ℓ and the matrix hydrides provide the source of hydrogen while the crack tip acts as a sink for hydrogen. The DFM was considered to make a small contribution but was included for completeness. Later the hysteresis of the solubility limit was included. The volume increase during hydride precipitation was invoked as the explanation for T_D and T_P being so far apart [20].

As an extension of this model, Kim [21] started with a temperature between T_D and T_P attained by cooling, T_Y in Fig. 3, so initially all the hydrogen is said to be in supersaturated solution. On the imposition of a tensile load on a specimen containing a crack, a hydride is postulated to nucleate at the crack tip. This precipitation is said to cause the supersaturation of hydrogen to decrease to C_D at

the stressing temperature. Thus a concentration gradient is set up between the crack tip (at C_D) and a region away from the crack, which contains the starting hydrogen concentration in supersaturated solution. This concentration gradient is said to be the driving force for DHC. This model is thus not new, but a variation on the initial Dutton and Puls model starting with all the hydrogen in solution. The DFM is categorically rejected by Kim as "an incredible assumption" [22].

In both versions of the PFM, the concentration of hydrogen in the bulk is greater than that at the crack tip. Both versions require that C_P be lowered by tensile stress. To date, no experimental evidence for such a reduction has been presented for zirconium alloys. The experimentally determined value of the partial molar volume of hydrogen in zirconium [23] implies that any effect of stress on solubility limits is small [24]. A theoretical treatment [25] also concluded that "solvi relations derived experimentally in unstressed solids can be used to a good approximation to determine the conditions at which hydrides will precipitate at ... crack tips". This evidence casts doubt on the importance, relevance and application of the precipitation first mechanism – PFM – as the correct model for the first step in DHC in zirconium alloys.

The DFM does not require the solvus to be changed by tensile stress. The DFM has been invoked to explain DHC when no hydrides are present in the zirconium matrix, T_Y in Fig. 3; on cooling, cracking was induced close to, but below T_D (Observation (b)) [26–28] while the DFM gave a satisfactory explanation for the effect of heating and cooling on DHC (Observation (e)) [29]. Also, Eq. (1) was followed, with no apparent change in Q, whether the starting microstructure contained hydrides, (T_X, Fig. 3), or not, (T_Y, Fig. 3) [30], thus the DFM has general application. In the DFM, the concentration of hydrogen in the bulk is lower than that at the crack tip, which is opposite to the PFM.

In this paper we discuss the DFM. Only the first step of DHC is considered. The rate of crack growth is assumed to be controlled by the rate of hydrogen arrival at the crack tip. We explain much of the phenomenology of DHC by DFM and discuss the rival models. The eventual suppression of cracking at very high temperaures [31] is discussed. No mechanisms of hydride fracture are discussed: no insight is offered on the initiation of cracking, K_{1H}.

2. Hydrogen diffusion under stress

A difference between the PFM and the DFM is that the former posits a concentration gradient as the 'driving force' for hydrogen movement, whereas hydrogen diffusion in the DFM happens because of a gradient in the chemical potential,[1] μ. The chemical-potential formalism is more general, and consistent with earlier findings that the tendency for particles to diffuse can be related to the chemical potential [33]: "gradients in chemical potential rather than concentration gradients are the fundamental motivating forces in diffusion" [34]; strictly speaking, a concentration gradient is not a force, having dimensions of mass × length^{-4}, but a gradient in a potential is a force, having dimensions of mass × length × time^{-2}. However, in the absence of applied stress, the DFM reduces to the PFM, so depending on the circumstances, the DFM and PFM can provide equivalent descriptions, as is shown below.

The DFM mathematical description for the movement of hydrogen in zirconium under stress can be formulated by solving the diffusion equation based on gradients of chemical potentials.

[1] "If to any homogeneous mass in a state of hydrostatic stress we suppose an infinitesimal quantity of any substance to be added, the mass remaining homogeneous and its entropy and volume remaining unchanged, the increase of the energy of the mass divided by the quantity of the substance added is the [chemical] potential for that substance in the mass considered" [32].

The flux of diffusing species (hydrogen), **J**, is defined as the product of their average velocity, $\hat{v}$, and their concentration, C:

$$\mathbf{J} \equiv \hat{v}C \tag{2}$$

Phenomenologically, the velocity is found to be proportional to a driving force.[2] The proportionality constant is called the mobility Γ, and the driving force is the gradient of the chemical potential, $\nabla\mu$, such that

$$\hat{v} = -\Gamma\nabla\mu \tag{3}$$

Hence, the phenomenological equation for the flux is [35]

$$\mathbf{J} = -\Gamma C\nabla\mu \tag{4}$$

This equation is the microscopic (continuum) form of Ohm's Law. The chemical potential [32] is defined as

$$\mu = \mu^\circ + RT\ln\ a \tag{5}$$

$$= \mu^\circ + RT\ln\ \gamma C \tag{6}$$

where a is the activity [36] of hydrogen in solution: $a = \gamma C$, where γ is the activity coefficient and C is the concentration of hydrogen in solid solution measured as a fractional amount (grams of hydrogen per gram of zirconium, expressed as parts-per-million by weight, or ppm) [37]. The reference state for the chemical potential, μ°, can be arbitrarily defined; in this study it is defined by the bottom (zero-point energy) of the potential well in which hydrogen sits in solid solution, which depends on stress.

The flux given by Eq. (4) is related to a diffusion constant when Fick's 1st empirical law [38] applies (*i.e.,* the flux depends linearly on the concentration gradient such that $\mathbf{J} = -D\nabla C$):

$$\mathbf{J} = -\Gamma C\nabla\mu = -D\nabla C \tag{7}$$

The relationship between diffusion constant and mobility is

$$\Gamma = \frac{D}{C}\left(\frac{\partial\mu}{\partial C}\right)^{-1} = D\left(\frac{\partial\mu}{\partial\ln\ C}\right)^{-1}. \tag{8}$$

Substituting Eq. (6) into Eq. (8) leads to the Einstein-Smoluchowski relation [39,40]

$$\Gamma = \frac{D}{RT} \tag{9}$$

Hence, Eq. (4) becomes

$$\mathbf{J} = -\frac{DC}{RT}\nabla\mu \tag{10}$$

Substituting the gradient of Eq. (6) into Eq. (10) yields, for isothermal conditions (*i.e.,* no temperature gradient), the general equation for the hydrogen flux in the absence of thermal gradients:

$$\mathbf{J} = -D\left(\nabla C + \frac{C}{RT}\nabla\mu^\circ + \frac{C}{\gamma}\nabla\gamma\right) \tag{11}$$

Eq. (11) is called the 'Nernst–Einstein' equation. The second term on the right-hand-side of Eq. (11), $(-DC/RT)\nabla\mu^\circ$, is called the 'drift term'.

For this paper, it is generally assumed that activity coefficients are the same at the crack tip and in the bulk and, hence, that there

[2] In general, velocity is not proportional to force: a constant force produces constant acceleration, for constant mass (Newton's Law), and this results in an ever-increasing velocity. However, velocity can be proportional to force for situations where the accelerated mass is continually colliding with surrounding material, for instance electrons in semiconductors, or hydrogen in zirconium jumping between interstitial sites in the lattice. If at each collision or jump the diffusing species stops, then the average 'drift' velocity will be equal to the acceleration due to the force, multiplied by the average time between collisions or jumps. Hence, the average drift velocity is proportional to the average time between collisions or jumps divided by the mass (which together is called the mobility) multiplied by the force, which is written as the negative gradient of a potential.

is no gradient in activity coefficients. This assumption is valid for dilute solutions in which the solute species do not interact. There are no reported activity coefficients for hydrogen in solution in zirconium so, for the present purpose, dilute is defined as less than 2 at% (≈200 ppm by weight), which is the concentration of hydrogen in solution in titanium above which activities were no longer linearly related to concentrations [41]. Titanium is a good comparator because it is in the same group as zirconium in the Periodic Table, and it has the same crystal structure and a similar partial molar volume for hydrogen.

A cross-sectional view of a crack is shown schematically in Fig. 4. Consider the case where initially there is no applied external stress on this crack, and the concentration of hydrogen in solution is everywhere the same (*i.e.,* the concentration gradient is zero at time zero). When tensile stress is applied to the crack, hydrogen flows to the stressed region directly in front of the crack from the unstressed bulk region far from the crack. The stress changes the potential-well depth, μ°, in which the hydrogen sits (Fig. 5), and causes a chemical potential gradient between the crack and the bulk. To compensate for the $\nabla\mu^\circ$, hydrogen flows, and a concentration gradient ensues. The hydrogen flows from the higher potential well in the bulk, to the lower potential well at the crack. The potential well is lower at the crack because there the tensile stress opens the lattice, thus making it easier to accommodate

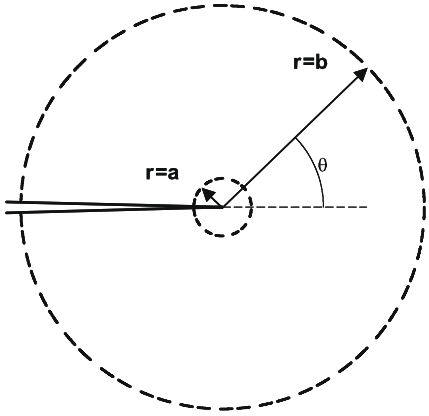

Fig. 4. A representation of the crack tip geometry.

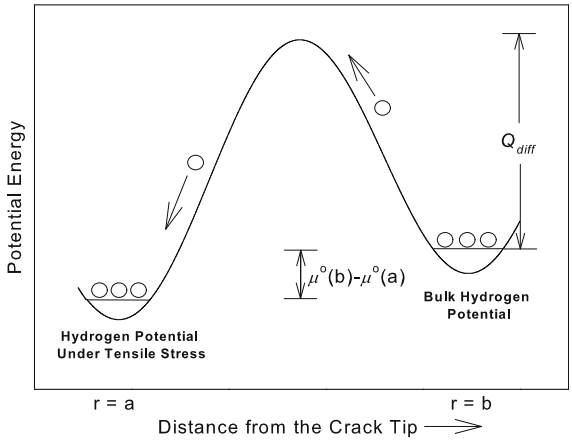

Fig. 5. A representation of how the chemical potential changes for hydrogen under stress at a crack tip relative to the bulk. If tensile stress is applied at a crack for which the initial hydrogen concentration is the same as in the bulk, then hydrogen (circles in the figure) flows from the bulk to the stressed region because of the chemical potential gradient. The barrier for diffusion $|Q_{diff}/R| \approx 4100$ K [42,43] is much larger than the potential energy drop because of the tensile stress at the crack tip: $(\mu^\circ(b) - \mu^\circ(a))/R$ equals 388 K at 20 °C and 248 K at 300 °C (Eq. (22)).

hydrogen atoms, so they are at lower potential energy. In the absence of an initial concentration gradient, the reason hydrogen moves to the stressed crack is because of the difference in the depths of the potential wells in the bulk and at the crack (*i.e.,* the drift term).

Hydrogen will cease to flow if equilibrium is reached, which is when the chemical potential gradient is zero. At this point, the chemical potential is the same everywhere, but getting to this point has produced a concentration gradient, ∇C, which is of opposite sign to the potential-well gradient, $\nabla\mu^\circ$, such that these terms in Eq. (11) cancel and the flux of hydrogen is zero (in the absence of an activity-coefficient gradient). Thus, hydrogen flows to the crack tip, because of the drift term, but this flow is opposed by the concentration gradient term, until the equilibrium concentration is reached. If the hydrogen concentration at the crack tip crosses the threshold to precipitate hydrides before it reaches the equilibrium concentration, then hydrides will precipitate at the crack tip. In this case, the concentration of hydrogen in solution in the vicinity of the crack will be at the terminal solid solubility precipitation limit: C_P, which is independent of stress in accord with experimental and theoretical evidence as explained in the introduction. Because C_P is below the equilibrium concentration, hydrogen will continue to flow from the unstressed bulk to the crack tip until the bulk hydrogen concentration decreases to the equilibrium value determined by equating the chemical potentials, Eq. (6), at $r = a$ and at $r = b$ (Fig. 4) (*i.e.,* $\mu_{r=a} = \mu_{r=b}$), or by equating the equation for the hydrogen flux, Eq. (11), to zero (*i.e.,* $\mathbf{J} = 0$), and solving for $C(b)$

$$C(b) = C_P(a)\frac{\gamma(a)}{\gamma(b)}\exp\left[\frac{\mu^\circ(a) - \mu^\circ(b)}{RT}\right] \tag{12}$$

However, cracking is not an equilibrium process. As hydrogen arrives at the crack tip, the hydride grows, and if and when the conditions are appropriate (*eg.,* $K_I > K_{IH}$, see Fig. 1), the hydride will crack (Observations (a), (c) and (d)). If the process of cracking the hydride is much faster than hydrogen diffusion (Observation (c)), then the crack-tip propagation is diffusion limited. The criteria for hydride cracking are not considered in this paper. It is sufficient for the current purpose to assume that the hydride can crack and that the continuous supply of hydrogen is sufficient to maintain the formation and growth of crackable hydrides (*i.e.,* $\mathbf{J} < 0$ because the hydrogen flux is from b to a). In this case, before equilibrium is reached, the crack tip has moved ahead to the end of the cracked hydride. The crack velocity can then be related to the hydrogen flux, with the crack-tip hydrogen concentration in solution at C_P. The hydrogen concentration in solution in the unstressed bulk will be at a value that depends on heating and cooling history, but for a propagating crack it will always be greater than the equilibrium value given by Eq. (12). The evolution of the hydrogen concentration in the bulk can be determined from Eq. (11) and mass-balance relations. A closed-form solution for the flux can be obtained with the assumption that the bulk hydrogen concentration in solution does not change during cracking. The hydrogen concentration in the bulk does not change significantly when small amounts of hydrogen move to the crack tip because the bulk is vast compared with the region around the crack tip – the ratio of the volume of the bulk of a typical specimen to the volume of the plastic zone and hydride at the crack tip is about 1000:1. In addition, as the hydride cracks, the crack tip moves to a region where the bulk concentration is always less depleted. Hence, the crack tip is at the TSSP concentration and the bulk is at a fixed value that depends on heating and cooling history. With the concentrations set at these fixed boundary values, there is no time dependence in the concentrations of hydrogen in solution (*i.e.,* steady-state conditions apply), hence from the continuity, or conservation of mass, equation,

$$\nabla \cdot \mathbf{J} = -\frac{\partial C}{\partial t} \tag{13}$$

the divergence of the flux equals zero, because $\partial C/\partial t = 0$.

Solving $\nabla \cdot \mathbf{J} = 0$ for the flux through a cylinder with inner and outer radii of a and b, respectively (see Fig. 4), yields

$$\mathbf{J} = \frac{-D \exp\left[\frac{\mu^\circ(b)-\mu^\circ(0)}{RT}\right]}{r\Phi}\left[C(b)\gamma(b) - C(a)\gamma(a)\exp\left[\frac{\mu^\circ(a)-\mu^\circ(b)}{RT}\right]\right] \tag{14}$$

where $\mu^\circ(0)$ is the potential-well depth at $r = 0$, and

$$\Phi = \int_a^b \gamma(r)\frac{\exp\left[\frac{\mu^\circ(r)-\mu^\circ(0)}{RT}\right]dr}{r} \tag{15}$$

Eq. (14) is the steady-state flux between a and b that is required to maintain constant concentrations $C(a)$ and $C(b)$; it depends on the hydrogen concentrations and the difference in the depths of the hydrogen potential wells at these radii. If the crack is under tension, then $\mu^\circ(a) < \mu^\circ(b)$ and the flux will be negative, that is, from b to a, and the hydrogen concentration will increase at the crack tip. If the region is under compression then the flux will be in the opposite direction.

The number of hydrogen atoms, dn, crossing the cylindrical boundary per time, dt, at radius r for an infinitely sharp crack (Fig. 4) whose velocity is limited by diffusion is

$$\frac{dn}{dt} = \int_0^{2\pi} d\theta r\mathbf{J} = 2\pi r\mathbf{J} \tag{16}$$

If cracking is limited by the rate of hydrogen reaching the crack tip, then the crack velocity will be proportional to dn/dt. Defining the proportionality constant as $k(T)$, to emphasize its temperature dependence, the crack velocity is

$$v_c(T) = \frac{k(T)2\pi D}{\Phi}\exp\left[\frac{\mu^\circ(b)-\mu^\circ(0)}{RT}\right] \times \left[C(b)\gamma(b) - C(a)\gamma(a)\exp\left[\frac{\mu^\circ(a)-\mu^\circ(b)}{RT}\right]\right] \tag{17}$$

Eq. (17) is the crack velocity under stress derived from the steady-state solution for the hydrogen flux. For a crack with no applied stress, and equal hydrogen concentration everywhere, there is no flux of hydrogen. If stress is applied to the crack, then initially the activity of hydrogen in solution is the same at the crack tip as it is in the bulk, because the hydrogen cannot move instantaneously. Hence, initially $C(a)\gamma(a) = C(b)\gamma(b)$, and the driving force for the hydrogen flux is the difference in the depths of the potential wells for hydrogen at the crack tip and in the bulk: $\mu^\circ(a) - \mu^\circ(b)$; if not for this difference, the large square bracket in Eq. (14) (and Eq. (17)) would be zero. This 'potential-energy' difference causes hydrogen to flow to the crack tip: the flux is negative (*i.e.*, $\mathbf{J} < 0$), and the crack tip acts as a sink where hydrogen in solution disappears as it becomes hydride. The steady-state solution for the hydrogen flux is appropriate when the volume of the bulk is much greater than the volume of the crack tip region, and when the 'potential-energy' difference is large enough so that hydrogen will flow until the concentration at the crack tip reaches the point where hydrides can nucleate, after which the concentration of hydrogen in solution will be at the TSSP value, where it remains as the hydride grows and cracks (if $K_I > K_{IH}$, see Fig. 1). In this case, the crack tip propagates with a velocity given by Eq. (17). The growth of the hydride limits the crack propagation, hence the connection between hydrogen flux and crack velocity. If the concentration of hydrogen in solution at the crack tip is not sufficient to cause precipitation there, or if the bulk concentration changes significantly as hydrogen accumulates at the crack tip, then the steady-state solution no longer applies, the solution is transient, and eventually equilibrium is reached: the concentrations of hydrogen in solution satisfy Eq. (12) (*i.e.*, $\mathbf{J} = 0$).

3. Some examples

Seven examples will be used to illustrate the DFM. The first three examples will require only equations for the temperature dependence of the yield strength, and TSSP as a function of temperature, but not stress, and a simple equation (Eq. (18)) derived from the definition that at equilibrium the chemical potentials of hydrogen in solution are the same everywhere. The last four examples will make use of the theory just developed for the crack velocity. These examples will explain the effect of heating and cooling histories depicted in Fig. 2.

3.1. Heat, load and cool without hydride precipitation: $T_4 - T_5$, Fig. 2

To illustrate the DFM, consider a cracked compact tension specimen of Zr–2.5Nb with bulk hydrogen concentration of 60 ppm heated to 340 °C, which is beyond the TSSD temperature of 302 °C, then put under tension, and then cooled, but not enough to precipitate hydrides. The concentrations in the bulk and at the crack are shown approximately in Fig. 6. Upon applying a tensile load to the crack, hydrogen diffuses to the crack tip from the bulk. The concentration of hydrogen at the crack tip can be written in terms of the bulk hydrogen concentration by rearranging Eq. (12):

$$C(a) = C(b)\frac{\gamma(b)}{\gamma(a)}\exp\left[\frac{\mu^\circ(b)-\mu^\circ(a)}{RT}\right] \tag{18}$$

The bulk concentration, $C(b)$, does not change appreciably remaining at 60 ppm as the specimen is cooled. When the crack-tip hydrogen concentration in solution reaches TSSP at T_5 (243 °C), hydrides can precipitate at the crack tip.

The potential energy difference for hydrogen in the bulk and at the stressed crack tip, $\mu^\circ(b) - \mu^\circ(a)$, can be estimated from small-strain deformation, elastic-plastic fracture mechanics theory [44]. If the material undergoing cracking behaves as a rigid body that deforms elastically, then an applied tensile stress would result in an infinite 'singular' stress at the crack tip. Slip-line theory resolves the singularity with a plastic zone in front of the crack tip that limits the stress to the yield strength for the material [45,46]. Because of conservation of energy, the pressure–volume work done on the

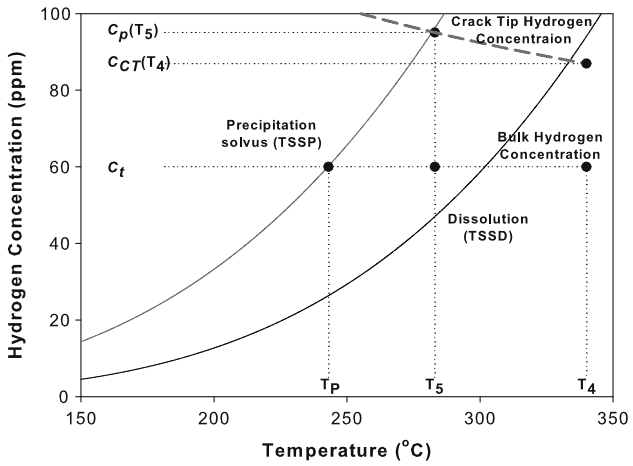

Fig. 6. The TSS lines for Zr–2.5Nb [14] and some points that are used in the text to illustrate the DFM (Section 3.1). Temperature T_4 and T_5 are the same as those in Fig. 2. The crack-tip hydrogen concentrations were calculated using Eq. (18) assuming the bulk concentration remains constant at C_t.

system when the tensile stress is applied is equal and opposite to the free energy change in the material, which per mole of hydrogen is [47]

$$\mu^{\circ}(b) - \mu^{\circ}(a) = -\sigma_h V_H \tag{19}$$

where V_H is the partial hydrogen molar volume (1.7×10^{-6} m^3/(mol(H) [23,48]) and σ_h is the hydrostatic pressure. The 'confining' hydrostatic pressure is negative for a tensile stress and is given by the trace of the stress tensor divided by three. The principal components for a Mode 1 plain-strain perfectly-plastic crack tip are given in Section 5.3.1 of [49], or in Eq. 2.85 in [50], from which the hydrostatic pressure can be derived in terms of the yield strength:

$$\sigma_h = -2.4\sigma_y \tag{20}$$

where σ_y is the yield strength, which for typical Zr–2.5Nb is given by

$$\sigma_y\ (\text{MPa}) = 810 - 1.02T\ (^{\circ}\text{C}) \tag{21}$$

which is based on data in [51]. Substituting Eqs. (20) and (21) into Eq. (19) and dividing by R, yields

$$\frac{\mu^{\circ}(b) - \mu^{\circ}(a)}{R} = 398 - 0.50T\ (^{\circ}\text{C}) \tag{22}$$

As an example, for a temperature of 250 °C,

$$\frac{\mu^{\circ}(b) - \mu^{\circ}(a)}{R} = 272\ \text{K} \tag{23}$$

The equilibrium concentration of hydrogen at the crack tip can be calculated as a function of temperature by substituting Eq. (22) into Eq. (18). Fig. 6 provides an example with a hydrogen concentration, C_T, of 60 ppm and with $\gamma(b)/\gamma(a) = 1$. At $T_4 = 340$ °C, the hydrostatic stress at the crack tip increases the hydrogen concentration in solution to $C_{CT}(T_4)$ (87 ppm). With further cooling, the crack-tip hydrogen concentration increases because σ_y increases; the hydrogen concentration at the crack tip follows the dashed "Crack Tip Hydrogen Concentration" line in Fig. 6. As the TSSD line shown in the figure is crossed at 302 °C, the hydrogen concentration in solution increases to 92 ppm, which is below TSSP. If cooling were stopped at this point, then no precipitates would form. At T_5 (283 °C), TSSP is reached as the crack-tip hydrogen concentration increases to $C_P(T_5)$, 95 ppm. For further cooling to T_P, the equilibrium hydrogen concentration at the crack tip calculated with Eq. (18) is above the TSSP concentration, as long as the bulk concentration remains at 60 ppm: strictly, during this cooling the concentration of hydrogen in solution in the bulk has decreased because hydrogen has moved to the crack tip. However, the change in concentration in the bulk is negligible because its volume is so much bigger than the region around the crack tip. The crack tip hydrogen concentration in solution cannot exceed the TSSP value, and hydrides can now precipitate at the crack tip. These conditions – the bulk concentration remainings constant and the crack-tip concentration being at TSSP – represent the steady state approximation leading to Eq. (14) for the hydrogen flux. As more hydrogen arrives at the crack tip, the hydride can grow. Eventually, the hydride could crack, if $K_I > K_{IH}$ (Fig. 1). Note that T_5 is 40 °C above the TSSP temperature, T_P, so that no hydrides are present in the bulk for this illustrative example.

Much experimental evidence is available to support this behaviour of hydrogen at a crack. Results from tests demonstrating hydride formation and cracking in Zircaloy and Zr–2.5Nb at temperatures between TSSD and TSSP are shown in Fig. 7. In the literature this temperature is called the "effective solvus temperature" [26] (see also Section 3.6) or T_5 [52,53], T_{RIT} [29,54] or T_{cr} [28]. These values were obtained by cooling cracked specimens and measuring the temperature at which cracking started under stress. The dashed line in Fig. 7 is the DFM prediction calculated following the method outlined above and in Fig. 6 for finding T_5, which is the onset temperature for cracking during cooling under stress.

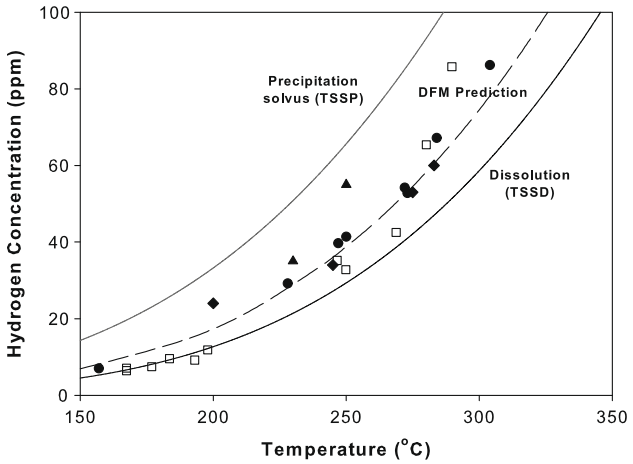

Fig. 7. The TSS lines for Zr–2.5Nb [14] and some data obtained by cooling cracked Zr–2.5Nb specimens under tensile stress and measuring the temperature at which cracking started: squares [26]; triangles [52]; circles [28]; diamonds are irradiated Zircaloy cracking data [29]. The dashed curve is the DFM prediction, which was calculated as described in Section 3.1.

3.2. Heat, cool to precipitate hydrides, and heat with load: $T_1 - T_3$, Fig. 2

A second illustrative example of the DFM is outlined in Fig. 8. In this example, cracked irradiated Zircaloy specimens are subjected to a tensile stress and heated from two different starting temperatures: T_1 equal to 25 and 200 °C. The hydrogen concentrations shown in the figure were calculated with Eq. (18) following the example in Section 3.1, but with the equations for TSSP, TSSD [13], and σ_y [29] for irradiated Zircaloy weld material. As the specimens depicted in the figure are heated, the hydrogen flux is initially negative (Eq. (11)), and hydrogen flows from the bulk to the crack tip; in accord with the steady-state approximation, the hydrogen concentrations in solution in the bulk remain fixed at the TSSP concentrations at the starting temperatures and appear as horizontal lines in Fig. 8. The crack-tip concentrations calculated with Eq. (18) are shown as dotted lines in the figure; on heating, these concentrations decline because σ_y is decreasing while the bulk concentrations remain constant. The hydrogen concentrations at the crack tip calculated with Eq. (18) are greater than the TSSP values, but the concentrations of hydrogen in solution at the crack tips cannot exceed TSSP, so they follow the TSSP line until a temperature is reached, T_3 ($\approx$ 122 °C for the lower starting temperature, and $\approx$ 243 °C for the higher starting temperature in the figure), at which point the hydrogen flux goes to zero; cracking slows down and eventually stops. If the temperature is increased above the arrest temperature, initially the hydrogen flux is positive as the concentration gradient term dominates the hydrostatic stress term in Eq. (11), and hydrogen flows to the bulk from the crack-tip hydride. Eventually, equilibrium is reached at which point the hydrogen flux is zero. Hydride growth and cracking cannot restart above the arrest temperature because $\mathbf{J} \geqslant 0$.

The temperature where cracking starts to slow down has been called T_{DAT} [54] and T_2 [53], and where it stops completely is called T_3 [53,52] and also sometimes T_{DAT} [29,55], this latter usage of T_{DAT} is preferred because crack arrest is easier to discern than the point of slowing down. These temperatures depend on the starting tem-

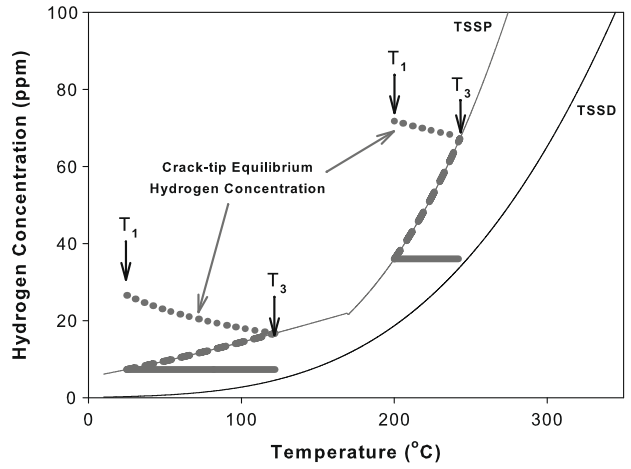

Fig. 8. The solid curves are the TSSP and TSSD lines for irradiated Zircaloy [13]. Two experiments are depicted in the figure. In both cases a cracked specimen with at least 36 ppm of hydrogen is heated to dissolve all of the hydrides and then cooled, in one instance to $T_1 = 25\,^{\circ}C$ and in the other to $T_1 = 200\,^{\circ}C$. The specimens are loaded and then heated again, as shown in the figure. The bulk hydrogen concentration in solution follows the solid horizontal lines. The crack-tip 'equilibrium' concentrations are shown as the dotted lines in the figure; they were calculated with Eq. (18) assuming the bulk concentration of hydrogen in solution remains constant, in accord with the steady-state approximation. The crack-tip concentrations cannot exceed TSSP, so as the specimens are heated the crack-tip concentrations follow the TSSP curve, as shown by the dashed lines in the figure. The flux of hydrogen is given by Eq. (11). Below T_3 the hydrogen flux is negative and hydrogen flows from the bulk to the hydrides. At T_3, the flux goes to zero, and at higher temperatures becomes positive so that hydrogen flows from the hydrides to the bulk.

perature, T_1, as long as it is low enough to cause precipitation (*i.e.*, below the TSSP temperature for the hydrogen concentration); the values estimated by experiment agree with those derived in the same way as in this illustrative application of the DFM, Fig. 9. In addition to the results on irradiated Zircaloy, data from cold-worked Zr–2.5Nb are included in Fig. 9. The difference in yield strength between the two materials is small and the predictions of T_3 are within the scatter of the data. Thus, we infer that TSSP for cold-worked Zr–2.5Nb is similar to that of irradiated Zircaloy at low temperatures (<170 °C). The data appear to be systematically above the predicted line in the figure, which suggests that

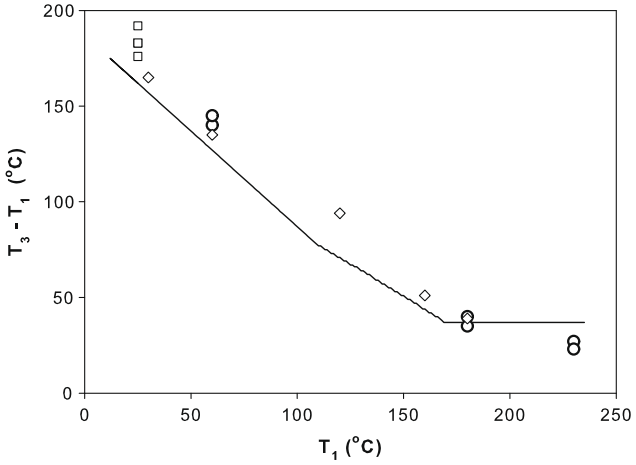

Fig. 9. The crack arrest temperature, T_3, upon heating from a minimum starting temperature, T_1. The line in the figure represents a simulation based on Eq. (18) and TSSP, TSSD and σ_y equations for irradiated Zircaloy, as discussed in Section 3.2; the open circles in the plot are for irradiated Zircaloy [29]. The data represented by the other symbols are for cold-worked Zr–2.5Nb: the squares are for cracks in the radial direction [54], and the diamond symbols represent cracks in the axial direction [55].

there may be hysteresis about the point where the cracking is predicted to stop and start. This hysteresis is discussed more in the next example in which the specimens are cooled, but not enough to cause precipitation in the bulk.

3.3. Heat, cool without hydride precipitation, and heat with load (following Section 3.1, then heat until cracking stops)

In this example, specimens of Zr–2.5Nb are heated so that all of the hydrogen is in solution, and then cooled through the dashed line in Fig. 7, but not low enough to cause precipitation in the bulk (*i.e.*, never below the TSSP temperature), and then reheated so that the dashed line in Fig. 7 is crossed. As the specimen is cooled it will start cracking when it first crosses the dashed line, and when it is reheated it will stop cracking when it crosses the dashed line again. The bulk concentration does not change during this heat-cool-heat cycle because the amount of hydrogen moving to the crack tip is small and the temperature never goes below the TSSP temperature. It is found experimentally that the crack initiation/arrest temperature is mainly *below* the TSSD temperature calculated with the TSSD equation given in [14]: Fig. 10 shows the predicted differences between the two, along with experimental results from [28]. The crack initiation temperatures on cooling are generally below the crack arrest temperatures on heating, which suggests, as in the previous example, that that there may be hysteresis about the temperature where the cracking is predicted to start and stop.

Initial attempts to explain results like these with the PFM were unsuccessful because the arrest temperatures were predicted to be *above* the TSSD temperatures rather than below as observed [18]. The correct sign and magnitude of the difference was obtained with a modified version of the PFM in which it was postulated that "the crack tip hydride is elastically highly constrained" [18]. In contrast, the agreement between observations and the DFM predictions can be seen in Fig. 10; the DFM predictions were calculated using only the equations for the temperature dependence of TSSP and yield strength given above, with no extra postulates required; the TSSD equation was used only to provide a reference temperature for the difference.

3.4. Cool from T_4 to precipitate various amounts of hydride, heat to a common test temperature

In temperature cycling experiments, cracking can be switched on by cooling and switched off by heating [56]. This effect can be

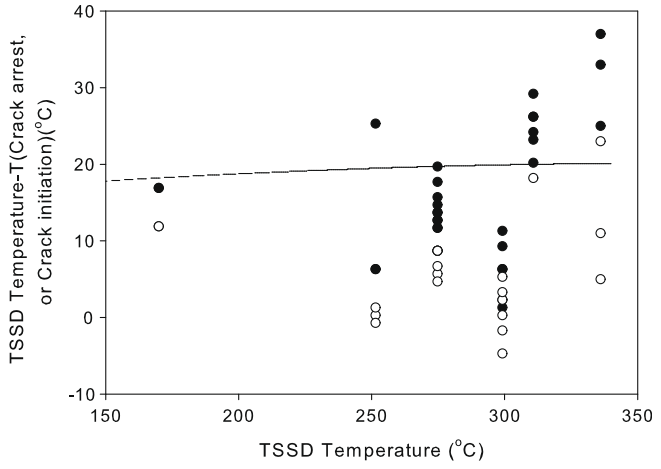

Fig. 10. The line in the figure represents a simulation based on TSSP, TSSD and σ_y equations for Zr–2.5Nb, as described in Section 3.3. The data represented by the filled circles are for cracking on cooling, and the open cirles are results for crack arrest upon heating [28].

exploited in reactor operation by temperature manoeuvres to minimize cracking [57]. In addition, temperature manoeuvres can be used to stimulate crack growth safely to aid in leak detection and location [58].

In the fourth illustrative example, we use the DFM to explain the effect of complicated thermal manoeuvres where specimens are heated to put all of the hydrogen into solution, then 'undercooled' to different temperatures (relative to the test temperature) to precipitate different amounts of hydrogen, and then heated to a common test temperature and loaded to the same amount. We use the experiments described by Kim [21] because he suggests that the results are "difficult to understand with the hypothesis that the stress gradient is a driving force for the DHC"; in other words, how does one obtain different crack velocities with various thermal histories using the same applied stress conditions?

3.4.1. Explaining the results by the DFM

The experimental specimens were Zr–2.5Nb with 60 ppm total hydrogen concentrations. These specimens were heated to 310 °C apparently for enough time to dissolve all of the hydrides, and then undercooled to 250, 240, 230, 220 and 210 °C, which is sufficient to begin hydride precipitation in all but for the first temperature. The temperatures of all of the specimens were then stabilized at 250 °C (which was the test temperature, T_t) and the same load (stress intensity factor of 15 MPa$\sqrt{\text{m}}$) applied to each, which led to cracking. The crack velocities were different, and depended on the amount of undercooling relative to the 250 °C test temperature. However, by design, each specimen was identically loaded; Kim is apparently suggesting that a stress-gradient model should predict no change in velocities, because the identical loading produces stress gradients that are the same for all specimens. The challenge is to explain how these undercooling results are consistent with the picture of hydrogen moving because of a stress gradient, which is the DFM developed in this paper. The answer can be given with reference to Eq. (11) where it can be seen that different hydrogen fluxes are expected for the same $\nabla\mu^\circ$ if the concentration gradients are different, as they are for the different undercoolings. However, $\nabla\mu^\circ$ is the same if the loads are all the same, or even if they are different because under any tensile stress the crack tip will always be at the yield strength (Section 3.1). The stress intensity factor relates to the applied stress and only needs to be large enough to crack the hydride.

For cracking experiments done at one temperature, $C(a)$ in Eq. (17) will be constant at the TSSP solubility limit for that temperature. The concentration of hydrogen in solution in the bulk, $C(b)$, will depend on the heating and cooling history. For the experiment, the values of $C(b)$ will be given by the TSSP equation for the various undercooling temperatures, T_{uc}, assuming the undercooling in each case was for sufficient time so that these values were reached. For the undercooling experiment, Eq. (17) is rewritten as

$$v_c(T_t) = {}^{\text{DFM}}W\left[C_{\text{P}}(T_{uc}) - C_{\text{P}}(T_t)\frac{\gamma(a)}{\gamma(b)}\exp\left[\frac{\mu^\circ(a)-\mu^\circ(b)}{RT_t}\right]\right] \tag{24}$$

where ${}^{\text{DFM}}W$, which implicitly depends on strength, is given by

$${}^{\text{DFM}}W = \frac{k(T_t)2\pi D\gamma(b)}{\Phi}\exp\left[\frac{\mu^\circ(b)-\mu^\circ(0)}{RT_t}\right] \tag{25}$$

Hence, a plot of velocity versus $C_P(T_{uc})$ will have slope ${}^{\text{DFM}}W$ and intercept

$$-\left({}^{\text{DFM}}WC_{\text{P}}(T_t)\frac{\gamma(a)}{\gamma(b)}\exp\left[\frac{\mu^\circ(a)-\mu^\circ(b)}{RT_t}\right]\right) \tag{26}$$

Fig. 11 shows Kim's reported velocities plotted versus their corresponding TSSP concentrations calculated at the undercooling temperatures from [14]:

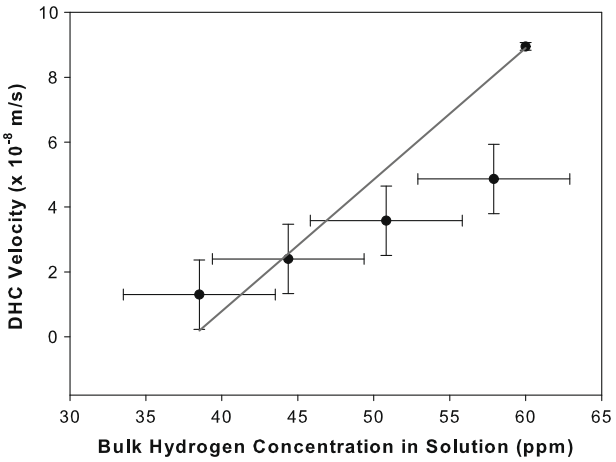

Fig. 11. Crack velocity data versus Hydrogen concentration in the bulk: the crack velocity data are from [21] and hydrogen concentrations in the bulk are calculated from Eq. (27) at the undercooling temperatures, with the exception of the 60 ppm value which is the total concentration in the sample. The ±5 ppm error bars in the concentrations are from [21]. The errors in the velocities are assumed to be equal to the standard deviations obtained from the distribution of 80 DHC velocity measurements made under the same conditions [30], with the exception of the 60 ppm error, which is the standard deviation divided by the square root of the number of observations. The velocities at 60 ppm in [21] and [30] are the same. The line in the plot was determined by least-squares regression with each datum weighted by the squared inverse of the assumed error. The line is consistent with Eqs. (24) or (34), where the slope and intercept are defined in the text depending on whether Eqs. (24) or (34) is used. The linearity of the plot ($r^2 = 0.9$) demonstrates that both the DFM and PFM provide a reasonable explanation of undercooling data.

$$C_P(T) = 4.11\times10^4\exp(-28000/8.314T)[\text{ppm}] \tag{27}$$

The linearity of the plot is reasonable ($r^2 = 0.9$) and hence the stress-gradient model (DFM) provides a reasonable description and explanation of the undercooling data.

The experimentally determined values for the slope and the intercept can be used to estimate the potential energy difference between the bulk and the crack tip. The parameter ${}^{\text{DFM}}W$ can be eliminated by taking the ratio of the intercept to the slope:

$$-C_{\text{P}}(T_t)\frac{\gamma(a)}{\gamma(b)}\exp\left[\frac{\mu^\circ(a)-\mu^\circ(b)}{RT_t}\right] \tag{28}$$

With $C_{\text{P}}(T_t)$ for $T_t = 250$ °C from Eq. (27), and assuming $\gamma(a)/\gamma(b) \approx 1$, then

$$\frac{\mu^\circ(a)-\mu^\circ(b)}{R} = -285\pm34\ \text{K} \tag{29}$$

This value compares well with the calculated potential energy difference, −272 K, for the test temperature of 250 °C (Eq. (23)).

3.4.2. Explaining the results by the PFM

In Kim's original paper [21] he simply presents the results and says they demonstrate his model: Kim claims that a strong correlation between the logarithm of the crack velocity and the amount of undercooling, or the difference in the hydrogen concentration between the bulk and the crack tip, confirms that concentration differences are the driving force for DHC. Here we use his conceptual picture and apply the appropriate analysis.

As a precursor to the PFM explanation of the undercooling experiment, Eq. (24) is rewritten in terms of an 'effective' concentration at the crack tip:

$$v_c(T_t) = {}^{\text{DFM}}W\left[C_{\text{P}}(T_{uc}) - {}^{\text{eff}}C^{\text{s}}_{\text{tip}}(T_t)\right] \tag{30}$$

where

$$^{\text{eff}}C^{s}_{\text{tip}}(T_t) = C_{\text{P}}(T_t)\frac{\gamma(a)}{\gamma(b)}\exp\left[\frac{\mu^{\circ}(a)-\mu^{\circ}(b)}{RT_t}\right] \tag{31}$$

These equations suggest that the crack velocity formula derived from the gradient of the chemical potential can be thought of in terms of concentrations, if the effect of the tensile stress at the crack tip is pictured to reduce the concentration of hydrogen in solution from C_{P} to an effective value $^{\text{eff}}C^{s}_{\text{tip}}$. However, care must be taken not to assign any undue physical significance to this 'effective' concentration.

There is no stress gradient in the PFM, so, in the absence of an activity-coefficient gradient, Eq. (11) reduces to

$$\mathbf{J} = -D\nabla C \tag{32}$$

Following the argument leading to the DFM velocity formula (Eq. (17)) (*i.e.*, solving $\nabla\cdot\mathbf{J}=0$ for the steady-state solution, integrating over the angular dependence and multiplying by the proportionality constant, $k(T)$ to give the crack velocity) the equivalent crack velocity based on a concentration gradient is

$$^{\text{PFM}}v_c(T_t) = \frac{k(T_t)2\pi D}{\ln(b/a)}(C(b)-C(a)) \tag{33}$$

which is Eq. (17) with all differences between μ° terms equal to zero, and where the activity coefficients are unity (see [59] for an alternate derivation of Eq. (33)).

In the PFM interpretation provided by Kim [21] for the the undercooling experiment, the bulk concentrations are 'supersaturated' at the TSSP values for the various undercooling temperatures, as in the DFM interpretation, but the crack tip is at the TSSD concentration, $^{\text{PFM}}C_{\text{D}}(T_t)$, because the applied stress has induced precipitation of the supersaturated hydrogen at the crack tip thereby lowering the concentration to the TSSD value. Thus,

$$^{\text{PFM}}v_c(T_t) = {}^{\text{PFM}}W(C_{\text{P}}(T_{uc}) - {}^{\text{PFM}}C_{\text{D}}(T_t)) \tag{34}$$

where

$$^{\text{PFM}}W = \frac{k(T)2\pi D}{\ln(b/a)} \tag{35}$$

which is Eq. (25) without stress, and thus with all differences between μ° terms equal to zero.

Eq. (34) has the same linear form as the corresponding equation for the DFM (Eq. (30)). Thus, the same plot of velocity versus $C^{P}(T_{uc})$ (Fig. 11) shows that the PFM could be used to describe the cracking data from undercooled specimens. (Note that the relationship is linear and not logarithmic as plotted by Kim [21].) The intercept divided by the slope should be equal to the PFM-TSSD concentration at 250 °C, which is also the concentration at zero crack velocity in Fig. 11,

$$^{\text{PFM}}C_{\text{D}}(250\,^{\circ}\text{C}) = 38 \pm 4\ \text{ppm} \tag{36}$$

This concentration is also the value obtained for the effective concentration at the crack tip calculated by Eq. (31). In addition, this point where the crack velocity goes to zero for the undercool-heat-load experiments (Eq. (36): 38 ppm at 250 °C) falls on the dashed line in Fig. 7, which shows where cracking will just start during cooling under load.

3.5. Crack velocities after heating, and cooling to above and below TSSP

In this fifth example of the DFM, the crack velocity formula developed in this paper will be used to show the Arrhenius-like behaviour upon cooling described by Eq. (1). Representative crack-velocity data from an international 'round-robin' study [30] are shown as filled circles in Fig. 12. These data were obtained by heating pre-cracked compact tension specimens of Zr–2.5Nb with seven total hydrogen concentrations ($C_t = 29, 31, 34, 38, 45, 58$, and 72 ppm) to temperatures well beyond the dissolution solvus temperatures, and then cooling to seven test temperatures ($T_t = 144, 162, 182, 203, 227, 250$ and 283 °C, respectively): the error bars in the plot represent standard deviations calculated from a total of 166 separate measurements. The specimens with the three highest concentrations were tested at temperatures that were above the TSSP temperatures (calculated with Eq. (27)) for the corresponding total hydrogen concentrations; the four lower concentration specimens were tested at temperatures that were below the TSSP temperature.

The data in Fig. 12 can be predicted with the DFM. Once cracking has begun, the hydrogen concentraion in solution at the crack tip will be at the TSSP value and, following Section 3.4, Eq. (17) can be rewritten as

$$v_c(T_t) = {}^{\text{DFM}}W\left[C(b) - C_{\text{P}}(T_t)\frac{\gamma(a)}{\gamma(b)}\exp\left[\frac{\mu^{\circ}(a)-\mu^{\circ}(b)}{RT_t}\right]\right] \tag{37}$$

The hydrogen concentration in solution in the bulk will depend on whether the test temperature, T_t, is above or below the TSSP temperature, T_{TSSP},

$$C(b) = C_t \quad \text{for } T_t > T_{\text{TSSP}} \tag{38}$$

$$C(b) = C_{\text{P}}(T_t) \text{ for } T_t < T_{\text{TSSP}} \tag{39}$$

Values for C_{P} are calculated by Eq. (27), which is also used to calculated T_{TSSP} for the various values of C_t. The value of $\mu^{\circ}(a) - \mu^{\circ}(b)$ for Zr–2.5Nb is given by Eq. (22). An estimate for $^{\text{DFM}}W$ at 250 °C is given by the slope of the line shown in (Fig. 11), as discussed in Section 3.4. Values for $^{\text{DFM}}W$ at other temperatures can be estimated using Eq. (25), with the assumption that the temperature dependence of the diffusion constant overwelms the temperature dependencies of the other terms in the equation. This approach is reasonable because the barrier for diffusion $|Q_{\text{diff}}/R| \approx 4100$ K [42,43] is much larger than the similar terms in Eq. (25) containing potential energy differences, which are expected to be in the range of a few 100 K (*eg.*, $\mu^{\circ}(b) - \mu^{\circ}(a) \approx 270$ K; see Fig. 5), which is well within the error for the value for the barrier.

The open circles in Fig. 12 show the predictions of the DFM (Eq. (37)). The DFM predictions are within two standard deviations of the mean experimental values for all but the lowest test temperature. (Thus justifying the assumption that the temperature depen-

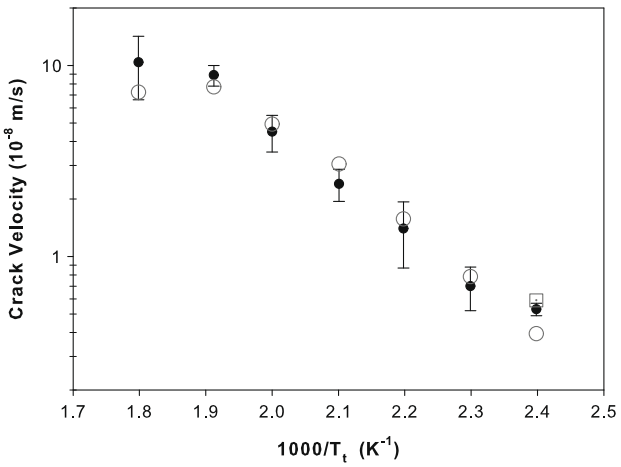

Fig. 12. Logarithm of crack velocity versus reciprocal temperature: the crack velocity data and their associated standard deviation errors are from [30]. The open circles are the DFM predictions, which are described in Section 3.5.

dence of ^{DFM}W is mostly determined by the temperature dependence of the diffusion constant.) The lowest temperature datum, for which $T_t = 144\,^{\circ}C$, is well below the temperature where the TSSP line for irradiated Zircaloy changed discontinuously at about 170 °C, as shown in Fig. 8. A similar discontinuous change is expected for Zr–2.5Nb based on the low temperature results shown in Fig. 9: the predictions for $T_3 - T_1$ do not rise for temperatures below 170 °C otherwise. If the crack velocity is estimated with the Zircaloy TSSP equation for temperatures below 170 °C [13], instead of Eq. (27), then the prediction at $T_t = 144\,^{\circ}C$ is shown as the open box in Fig. 12.

The data and DFM predictions plotted in Fig. 12 show a general negative linear trend when the logarithm of the crack velocity is plotted versus reciprocal temperature, which is in accord with the general Arrhenius form (Eq. (1)). The DFM predictions and the experimental observations are both consistent with an apparent activation energy for DHC of $Q = 47$ kJ/mol. However, the DFM shows that an Arrhenius dependence is not always to be expected, as can be seen from the prediction for the highest temperature datum in Fig. 12. This predicted velocity is less than the predicted velocity at the next lower temperature. For instances when the test temperature is above T_{TSSP}, the crack velocity is very sensitive to the difference between T_t and T_{TSSP}: as the difference increases, the crack velocity decreases (and eventually goes to zero) because the concentration gradient that opposes hydrogen flowing to the crack tip increases. Thus, depending on the choice of test temperature relative to precipitation temperature, the crack velocity could exhibit very non-Arrhenius behaviour, which could look like a high-temperature DHC limit, for example.

An example of high-temperature non-Arrhenius behaviour is expected between T_5 and T_6 in Fig. 2 and is shown in Fig. 13 [52]. These data were obtained from single specimens of the same material as in Fig. 12 that were heated to put all of the hydrogen into solution, and then cooled and the crack velocity measured, and then reheated again to put all of the hydrogen into solution, and cooled again to a different temperature and the crack velocity measured. This procedure was repeated several times. In the work described in Fig. 12, only one crack-velocity measurement was made per specimen: the specimens were not reheated and cooled again; the single-specimen method tends to produce lower values of v_c. The crack-velocity predictions shown in Fig. 13 were calculated with the TSSP2 equation given in the Ref. [52], rather than Eq. (27), because the TSSP2 equation is consistent with the TSSD line on which DSC measurements of samples taken from these specimens fall (see Fig. 5 of [52]). Although the crack velocities are generally underpredicted, predicted values of the T_5 (onset) and T_6 (peak) temperatures agree with the observations.

Crack velocity predictions based on Eq. (27) were not nearly as good, which emphasizes the sensitivity of the predictions to TSSP, especially when predicting crack arrest temperatures which require accurate small differences between large terms in the velocity equations given above. TSS of Zr–2.5Nb changes with heat-treatment because of the decomposition of the β-Zr phase [60]. Eq. (27) [14] provides an average value. For determinations of DHC velocities, as in this example, accurate and appropriate values of TSSP are required.

3.6. Incubation times

Time is required to build up the hydrogen concentration at the crack tip to reach the critical condition to crack the hydride [61]. This incubation time can be detected by onset of acoustic emission, or deviations in potential drop accompanying crack opening. The striations that are observed on the fracture surface after DHC in Zr–2.5Nb have been interpreted as representing cracked hydride [62]. In principle one can estimate the expected incubation time by dividing the striation spacings by the crack velocity. Using the observed values of striation spacing [30] and the calculated values of crack velocity (Section 3.5) we find that the predicted incubation times are close to the mean values observed using potential drop, and follow the same temperature dependence, with a notable increase at the highest test temperature, Fig. 14. The spread of observed incubation times is large because the sensitivity of some test equipment was insufficient to resolve the starting point of cracking and variation in preparation of the starting crack could affect its initial stress distribution.

The above interpretation can be extended to temperatures close to T_5 (Fig. 2), as shown by the dotted line in Fig. 15. In this example, the incubation times were measured by acoustic emission [26,27]. The specimen contained a mixture of hydrogen and deuterium (46 ppm equivalent total hydrogen) and cracking was observed in what was originally the radial direction of a Zr–2.5Nb pressure tube. Scaling the predicted incubation times by the ratio of the axial to radial crack velocities in the temperature range of the tests [14] and using a diffusion constant $\sqrt{2}$ times smaller to account for the mainly deuterium solute, provides a close prediction of

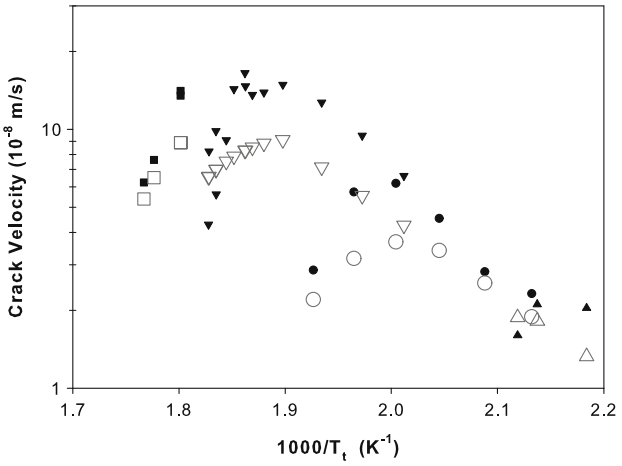

Fig. 13. Demonstration of T_5 and T_6 (Fig. 2) with crack velocity measured during cooling from T_4. The crack velocity data are shown as filled symbols for four total hydrogen concentrations: 24 (up-triangles), 34 (circles), 53 (down-triangles) and 60 ppm (squares) [52]. The open symbols are the DFM predictions, which are described in Section 3.5.

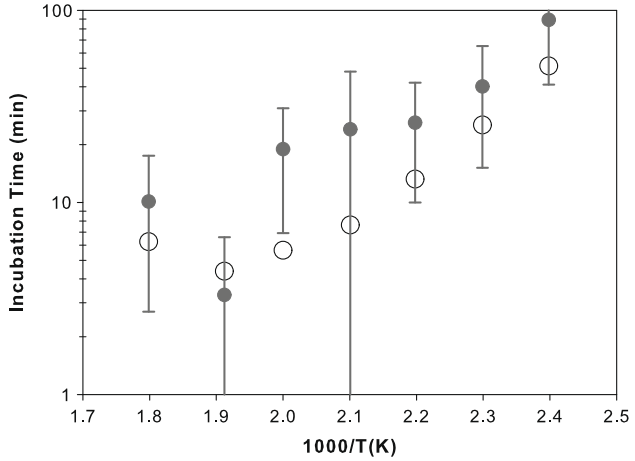

Fig. 14. Mean incubation times for Zr–2.5Nb DHC shown as filled circles with their associated standard deviation errors from [30]; the corresponding crack velocities are shown in Fig. 12. The open circles show the predictions, which are described in Section 3.6.

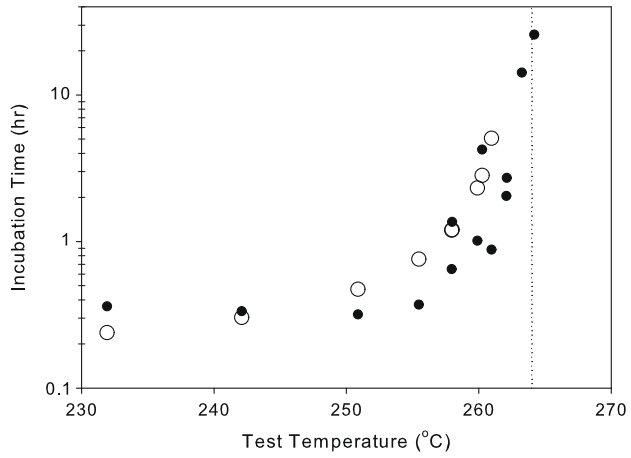

Fig. 15. Temperature dependence of incubation times for Zr–2.5Nb DHC showing increase in incubation time when the temperature is close to the effective solubility limit - dotted line - from [27], filled circles. The open circles show the predictions, which are described in Section 3.6.

the observed behaviour, Fig. 15. Close to T_5 the incubation time increases until a temperature is reached where no cracking is possible – in the experiments no cracking was observed after waiting for 50–90 h. This observation led to calling this temperature the "effective" TSSD temperature [26], as discussed in Section 3.1. This temperature corresponds to the point on the dashed line in Fig. 7 where the total hydrogen concentration is 46 ppm.

The observation of striations in post-test examinations of cracks is evidence that the crack front moves by discontinuous cracking events [62,63] (Observation (c)). Figs. 14 and 15 show the agreement of observed incubation times with times determined from striation lengths divided by crack velocities calculated from diffusion theory: the steps are large and quickly taken, but each step is delayed by hydrogen diffusion, so that the crack velocity is diffusion limited. This consistency between step length, velocity and time supports the contention in Section 2 that diffusion controls DHC velocity.

3.7. High-temperature DHC limit

As the test temperature is increased, the steady-state solution will become progressively less applicable. The flux can be so large that the bulk is readily depleted and the requirements for steady state no longer exist. The flux increases at higher temperatures because the diffusion constant increases with temperature, and because at high temperatures the concentrations of hydrogen in solution at the crack tip and in the bulk become large enough so that their associated activity coefficients are no longer equal, and an activity-coefficient gradient further enhances diffusion from the bulk to the crack tip via the last term on the right-hand-side of Eq. (11). Activity coefficients are not known for zirconium. For titanium, activity no longer increases linearly with concentration above 2 at% hydrogen in solution [41]. If zirconium behaves like titanium, then enhanced diffusion because of an activity-coefficient gradient would be expected to occur above 370 °C, which is the Zircaloy TSSP temperature for 2 at% (220 ppm) hydrogen in solution [13]; higher temperatures (≈30–60 °C, depending on heat treatment) are expected for Zr–2.5Nb because of partioning of hydrogen to the β-Zr phase.

Even though steady-state conditions do not apply at high temperatures, hydride is still precipitated at the crack tip, as long as the crack-tip concentration calculated with Eq. (18) is above the TSSP value, however, as the bulk concentration declines the flux towards the crack tip decreases until equilibrium is reached and the flux is zero. At equilibrium, the hydrogen concentration in solution at the crack tip is given by the TSSP value, and the bulk hydrogen concentration in solution is given by Eq. (12), although whether equilibrium is reached before cracking will depend on the stress intensity factor. For higher temperatures, the bulk hydrogen concentration in solution will decrease even faster, so the time to make hydride before equilibrium is reached is even shorter, so the net hydride production is less. Thus, in the high-temperature limit where the steady-state approximation no longer applies, the length of the hydride at the crack tip will be limited by the time to get to equilibrium, which is shorter for higher temperatures. Thus, a progressively greater K_I will be required at these higher temperatures to initiate cracking of the crack-tip hydride. Thus, K_{IH} will increase, and when it is greater than the applied stress intensity factor, cracking will stop. Alternatively, cracking could stop at these higher temperatures if equilibrium is reached because the flux goes to zero: no flux, no cracking. Also, the stress at the crack tip could be relaxed by creep resulting in a stress insufficient to fracture the crack-tip hydrides [64].

High-temperature crack velocities are shown in Fig. 16 [64]. These data were obtained by heating to dissolution and then cooling to the test temperature. The predictions derived from the steady-state solution (Section 3.4) are shown as open circles in the figure. The steady-state solution does not agree well with the observed crack velocities at high temperature. This observation is consistent with the experimental observation that K_{IH} increased for these data beyond the stress intensity factor for the applied loads [63,64]. Similar high-temperature data have been observed for Zircaloy-4 [65], and likewise predictions made with the steady-state solution do not match well above the high-temperature DHC limit, which happens at approximately 300 °C for Zircaloy-4 (c.f. ≈350 °C for Zr–2.5Nb, Fig. 16) [65].

4. Discussion

This paper describes a diffusion-based model for the mechanism of DHC in zirconium alloys where the first step in the process is the accumulation of hydrogen at the high tensile-stress region at a crack tip. This process is driven by the (negative) gradient in chemical potential, $\nabla\mu$; when the stress is applied the chemical potential is lowered at the crack tip relative to the bulk of the material away from the crack tip. This gradient has the units of a force and is able to move hydrogen in the metal lattice. If no hydride precipitation intervenes, eventually the flux of hydrogen, **J**,

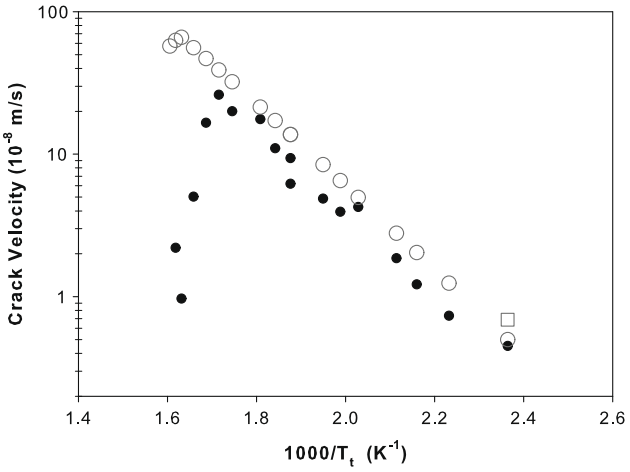

Fig. 16. Decline in crack velocity for Zr–2.5Nb at high temperatures: The measured crack velocities are shown as filled symbols [64]. The open symbols are the DFM predictions, which are described in Section 3.7. No cracking is observed above the high-temperature limit at ≈350 °C.

goes to zero as μ is equal everywhere; equilibrium is established. The hydrogen concentration is greater at the crack tip than in the bulk. The hydrogen concentration gradient exactly opposes the stress-induced hydrogen movement to the crack tip. Experiments have demonstrated that this process of hydrogen migration in a stress gradient is measurable. As examples:

- the hydrogen concentration decreased in vanadium, tantalum and niobium under hydraulic pressure [66] as expected from Eq. (14) because $\mu^{\circ}(a) > \mu^{\circ}(b)$ for compressive stress;
- with high tensile stresses hydrogen concentration increased in 4340 steel [67],
- in titanium alloys the equilibrium pressure of hydrogen at 600–800 °C changed as the material was stressed in tension and compression. Tension decreased the activity while compression increased it; torsion had no effect [41], which suggests that hydrostatic stress rather than deviatoric stress is responsible for changes in activity.
- in Zr–2.5Nb subject to bending the hydrogen moved from the region under compression to that in tension [48], having attained equilibrium.

Further corroboration for this theory was that values of hydrogen partial molar volume, V_H, determined from an analysis in terms of chemical potentials, from these stressing experiments agreed with those derived directly from measurements of changes in lattice parameter by hydrogen in solution (see in Refs. [41,48,66,67]). A beautiful non-hydrogen example can be found in the experiments of Darken on the diffusion of interstitial carbon between iron alloys [68]. There is no applied stress in these experiments, but they show that movement of solute is due to the gradient of the chemical potential and not the gradient of the concentration.

If the amount of hydrogen accumulated at the crack tip is sufficient to exceed the terminal solid solubility limit for precipitation (TSSP) then hydrides form. The flux of hydrogen is negative, and hydrogen flows from the bulk to the crack tip, thus growing the hydride that forms there. As a result, the bulk concentration will decrease although its volume is so much greater than that of the highly stressed region that its concentration remains essentially constant as the crack propagates. With the hydrogen concentration in solution in the bulk at some constant value, and the crack tip at the TSSP limit, a steady state ($\partial C/\partial t = 0$) is postulated to develop as the hydride grows.

In Zr–2.5Nb a striation results when a crack extends by DHC. Simultaneous monitoring of cracks by acoustic emission and potential drop shows that cracking proceeds in a series of jumps. In specially prepared specimens these jumps exactly corresponded with each other and to the fracturing of hydrides and the formation of striations [69]. This part of the process of DHC is therefore a sudden and fast event. The interpretation was that the rate of cracking of hydride is much faster than the rate of accumulation of hydrogen to renew the hydride and, thus, it is this accumulation of hydrogen that controls the rate of the development of the delayed hydride crack: DHC is limited by the diffusion of hydrogen to the crack tip under the influence of a (negative) chemical potential gradient that results when a tensile stress is applied to the crack tip. The diffusion first model developed in this paper describes the DHC velocity in terms of a steady-state diffusion flux. This model contains no criteria for hydride fracture: a description of K_{IH} is beyond the scope of this model since this phenomena depends on modeling cracking, not just hydrogen accumulation. In the preceding sections, the diffusion first model successfully describes the effects of the main variables, especially temperature history, on crack velocity.

In a series of papers Kim [21,22,70–77] has criticized this diffusion first model on the following grounds:

1. *The amplification of the hydrogen concentration at a crack tip was said to be insufficient to precipitate hydrides [21]*
   The amplification by stress is insufficient to form hydrides when the concentration of hydrogen in solution is at the TSSD value at the temperature for TSSD, T_D, as claimed in [21]. However, at some temperature lower than T_D, TSSP can be exceeded through the stress amplification well before the temperature for TSSP, T_P, is reached. In this paper, this temperature is identified by the dashed line in Fig. 7, which also shows some of the results of experiments that demonstrate the point, thus the criticism of Kim is refuted.
2. *The DFM cannot predict the temperature dependence of DHC, especially the effects of heating and cooling.*
   The seven examples in Section 3, comprising 15 independent data sets, provide ample demonstration that the DFM describes the experimental data, including the effects of temperature cycling.
3. *The DFM cannot provide a rationale for the constant DHC velocity independent of stress intensity factor*, K_I.
   The independence of DHC velocity with K_I is shown schematically in Fig. 1 by the stable-crack growth portion of the curve between K_{IH} and K_{IC}. The stress intensity factor for Type I cracking is proportional to the product of the applied stress and the square root of the crack length [49,50]; neither the stress intensity factor, nor the applied stress, nor the crack length, appear in the DFM DHC-velocity equations presented in this paper. Thus, in a trivial way, the DFM is independent of K_I.
   However, the DFM is not independent of hydrostatic stress. Any applied tensile stress at the crack plastically deforms a small region close to the crack tip. The resulting stress in the plastic zone is limited by the peak hydrostatic stress, which is equal to 2.4 times the yield strength (for a Mode I crack), which is independent of the load on the component. The hydrostatic stress changes the local depth of the potential well for hydrogen in solution, and thus governs the hydrogen accumulation rate and subsequent hydride growth rate, independent of K_I.

This paper answers Kim's criticisms.

In Section 3.4.2, by setting all the differences between μ° terms to zero in the DFM velocity equation, we obtained an equivalent velocity equation for PFM. Both velocity equations equally well represent the data shown in Fig. 11, thus these data cannot be used to prove or refute either picture. The conclusion that stress gradients play no role in DHC [21] cannot be made based on these data. Even though the models cannot be distinguished in this example, it would be incorrect to infer that they were somehow equivalent. The PFM picture relies on precipitation as the first step, and there is no experimental or theoretical evidence for this assumption. Such a process has to be demonstrated before any credence can be placed on the PFM. The proposed DFM is robust and with no unrealistic or unsupported assumptions. It is corroborated by the independent observations of the movement of hydrogen in stress gradients in several materials, including zirconium. It depends on well-characterized and independently-measured variables, such as the solubility limit, yield strength, diffusivity, and partial molar volume of hydrogen in zirconium, and it quantitatively describes many experimental observations.

5. Conclusion

The two main models for DHC of zirconium alloys are distinguished by their first step: either hydride precipitates at the crack tip immediately on loading – the precipitate first model (PFM) – or a flux of hydrogen is driven to the crack tip by the force generated by the difference in chemical potential for hydrogen at the crack

tip and the bulk material – the diffusion first model (DFM). The DFM postulates that the hydrogen concentration at the crack tip becomes greater than that in the bulk material. A hydride forms once the terminal solid solubility for precipitation (TSSP) is exceeded. In this paper, the DFM has been used to describe quantitatively seven independent experimental observation sets, using independently measured values of TSSP, yield strength, diffusivity, and partial molar volume of hydrogen in zirconium.

Note added in proof

During the preparation of this paper the authors became aware of a paper by M.P. Puls [78] one of the purposes of which was to provide an updated version for the model for DHC as originally proposed by Dutton and Puls [16–19] by using the sign convention for tensile stress used in later versions of the model. This paper demonstrated the physical incorrectness of a model for DHC propagation proposed recently by Kim and co-workers [21,22,71–77]. It also provides a rebuttal to their model in which it is suggested that hydrogen movement down a gradient of chemical potential is irrelevant and spontaneous and preferential precipitation of hydride at the crack tip upon load application is the first step for each successive stage of DHC.

References

[1] E.C.W. Perryman, Nucl. Energy 17 (1978) 95–105.
[2] P.A. Platonov et al., The study of cause of cracking in zirconium alloy channel tubes, Poster Paper at ASTM Zirconium in the Nuclear Industry – Eighth International Symposium, available as AECL Report RC-87, 1988.
[3] K. Edsinger, J.H. Davies, R.B. Adamson, Degraded fuel cladding fractography and fracture behaviour, in: G.P. Sabol, G.D. Moan (Eds.), Zirconium in the Nuclear Industry – Twelfth International Symposium, ASTM STP 1354, American Society for Testing and Materials, West Conshohocken, PA, 2000, pp. 316–339.
[4] C.E. Coleman, G.L. Doubt, R.W.L. Fong, J.H. Root, J.W. Bowden, S. Sagat, R.T. Webster, Mitigation of harmful effects of welds in zirconium alloy components, in: A.M. Garde, E.R. Bradley (Eds.), Zirconium in the Nuclear Industry – Tenth International Symposium, ASTM STP 1245, American Society for Testing and Materials, Philadelphia, 1994, pp. 264–284.
[5] C.E. Coleman, Cracking of hydride-forming metals and alloys, comprehensive dtructural integrity, in: J. Petit, P.M. Scott (Eds.), Environmentally Assisted Failure, vol. 6, Elsevier Ltd., Oxford, UK, 2003, pp. 103–161 (Chapter 6.03).
[6] C.E. Coleman, J.F.R. Ambler, Rev. Coatings Corros. 3 (1979) 105–157.
[7] D.O. Northwood, U. Kosasih, Int. Metals Rev. 28 (1983) 92–121.
[8] R.L. Eadie, R.R. Smith, Can. Metall. Quart. 27 (1988) 213–223.
[9] A. Sawatzky, C.E. Ells, Understanding hydrogen in zirconium, in: G.P. Sabol, G.D. Moan (Eds.), Zirconium in the Nuclear Industry – Twelfth International Symposium, ASTM STP 1354, American Society for Testing and Materials, West Conshohocken, PA, 2000, pp. 32–48.
[10] W.H. Erickson, D. Hardie, J. Nucl. Mater. 13 (1964) 254–262.
[11] G.F. Slattery, J. Inst. Metals 95 (1967) 43–47.
[12] Z.L. Pan, I.G. Ritchie, M.P. Puls, J. Nucl. Mater. 228 (1996) 227–237.
[13] A. McMinn, E.C. Darby, J.S. Schofield, The terminal solid solubility of hydrogen in zirconium alloys, in: G.P. Sabol, G.D. Moan (Eds.), Zirconium in the Nuclear Industry – Twelfth International Symposium, ASTM STP 1354, American Society for Testing and Materials, West Conshohocken, PA, 2000, pp. 173–195.
[14] Canadian Standards Association, Technical Requirements for In-service Evaluation of Zirconium Alloy Pressure Tubes in CANDU Reactors, N285.8-05, 2005.
[15] C.J. Simpson, C.E. Ells, J. Nucl. Mater. 52 (1974) 289–295.
[16] R. Dutton, M.P. Puls, A theoretical model for hydrogen induced sub-critical crack growth, in: A.W. Thompson, I.M. Bernstein (Eds.), Proceedings of Effect of Hydrogen on Behavior of Materials, Metal Society, AIME, New York, 1976, pp. 516–528.
[17] R. Dutton, K. Nuttall, M.P. Puls, L.A. Simpson, Metall. Trans. 8A (1977) 1553–1562.
[18] L.A. Simpson, M.P. Puls, Metall. Trans. 10A (1979) 1093–1105.
[19] M.P. Puls, L.A. Simpson, R. Dutton, Hydride-induced crack growth in zirconium alloys, in: L.A. Simpson (Ed.), Fracture Problems and Solutions in the Energy Industry, Pergamon Press, Oxford, 1982, pp. 13–25.
[20] M.P. Puls, Acta Metall. 32 (1984) 1259–1269.
[21] Y.S. Kim, Metals Mater. Int. 11 (2005) 29–38.
[22] Y.S. Kim, S.B. Ahn, Y.M. Cheong, J. Alloys Cmpd. 429 (2007) 221–226.
[23] S.R. MacEwen, C.E. Coleman, C.E. Ells, J. Faber Jr., Acta Metall. 33 (1985) 753–757.
[24] R.L. Eadie, C.E. Coleman, Scr. Metall. 23 (1989) 1865–1870.
[25] M.P. Puls, B.W. Leitch, S.-Q. Shi, The effect of applied stress on the accommodation energy and the solvi for the formation and dissolution of zirconium hydride, in: N.R. Moody, A.W. Thompson, R.E. Ricker, G.S. Was, R.H. Jones (Eds.), Hydrogen Effects on Material Behavior and Corrosion Deformation Interactions, The Minerals, Metals & Materials Soc., 2003, pp. 233–248.
[26] C.E. Coleman, J.F.R. Ambler, Can. Metall. Quart. 17 (1978) 81–84.
[27] C.E. Coleman, J.F.R. Ambler, Scr. Metall. 17 (1983) 77–82.
[28] S.-Q. Shi, G.K. Shek, M.P. Puls, J. Nucl. Mater. 218 (1995) 189–201.
[29] J.S. Schofield, E.C. Darby, C.F. Gee, Temperature and hydrogen concentration limits for delayed hydride cracking in irradiated Zircaloy, in: G.D. Moan, P. Rudling (Eds.), Zirconium in the Nuclear Industry – Thirteenth International Symposium, ASTM STP 1423, American Society for Testing and Materials, West Conshohocken, PA, 2002, pp. 339–357.
[30] C.E. Coleman, V.V. Inozemtsev, J. ASTM Int. 5 (2008). Paper JAI101091.
[31] R.R. Smith, R.L. Eadie, Scr. Metall. 22 (1988) 833–836.
[32] J.W. Gibbs, On the equilibrium of heterogeneous substances, Trans. Connecticut Academy. III (1875/6) 108–248 (the "intrinsic potential" of Gibbs would later be called the chemical potential by W.D. Bancroft, see A. Ya. Kipnis,"J.W. Gibbs, and chemical thermodynamics", in: K. Martinas, L. Ropolyi, P. Szegedi (Eds.), Thermodynamics: History and Philosophy: Facts, Trends, Debates, World Scientific, Singaport, 1991, p. 499.)
[33] J.C. Maxwell, Speaking to a conference of British chemists in 1876, in: E. Garber, S.G. Brush, C.W.F. Everitt, Maxwell on Heat and Statistical Mechanics: On "Avoiding All Personal Enquiries" of Molecules Lehigh U.P., Bethlehem, PA, 1995, p. 259.
[34] J. Bardeen, C. Herring, Diffusion in Alloys and the Kirkendall Effect, in: Imperfections in Nearly Perfect Crystals, Wiley, 1952, pp. 261–288.
[35] C.P. Flynn, Point Defects and Diffusion, Clarendon Press, Oxford, 1972.
[36] G.N. Lewis, Proc. Am. Acad. 43 (1907) 259;
G.N. Lewis, Z. Phys. Chem. 61 (1907) 129.
[37] International Union of Pure and Applied Chemistry, Quantities, Units and Symbols in Physical Chemistry, second ed., Blackwell Science, Oxford, 1993, pp. 4950, ISBN:0-632-03583-8.
[38] A. Fick, Philos. Mag. 10 (1855) 30.
[39] A. Einstein, Ann. Physik. 322 (1905) 549–560.
[40] M. von Smoluchowski, Ann. Phys. 326 (1906) 756–780.
[41] J.L. Waisman, G. Sines, L.B. Robinson, Metall. Trans. 4 (1973) 291–302.
[42] A. Sawatzky, J. Nucl. Mater. 2 (1960) 62–68.
[43] A. Sawatzky, G.A. Ledoux, R.L. Tough, C.D. Cann, Hydrogen diffusion in zirconium–niobium alloys, in: T.N. Vezroglu (Ed.), Proeedings of International Symposium on Metal-hydrogen Systems, Pergamon Press, Miami Beach, FL, 1982, pp. 109–120.
[44] J.W. Hutchinson, Nonlinear Fracture Mechanics, Department of Solid Mechanics, The Technical University of Denmark, 1979.
[45] J.W. Hutchinson, J. Mech. Phys. Solids 16 (1968) 13–31.
[46] J.R. Rice, G.F. Rosengren, J. Mech. Phys. Solids 16 (1968) 1–12.
[47] J.C.M. Li, R.A. Oriani, L.S. Darken, Z. Phys. Chem. Neue Folge 49 (1966) 271–279.
[48] R.L. Eadie, K. Tashiro, D. Harrington, M. Leger, Scr. Metall. Mater. 26 (1992) 231–236.
[49] M.F. Kanninen, C.H. Popelar, Advanced Fracture Mechanics, Oxford University Press, 1985.
[50] K. Hellan, Introduction to Fracture Mechanics, McGraw-Hlll Book Company., New York, 1985.
[51] C.E. Coleman, J.F.R. Ambler, Susceptibility of Zirconium alloys to delayed hydrogen cracking, in: A.L. Lowe Jr., G.W. Parry (Eds.), Zirconium in the Nuclear Industry, ASTM STP 633, American Society for Testing and Materials, Philadelphia, PA, 1977, pp. 589–607.
[52] P. Cirimello, G. Domizzi, R. Haddad, J. Nucl. Mater. 350 (2006) 135–146.
[53] B.A. Cheadle, C.E. Coleman, J.F.R. Ambler, Prevention of delayed hydride cracking in zirconium alloys, in: R.B. Adamson, L.F.P. Van Swam (Eds.), Zirconium in the Nuclear Industry – Seventh International Symposium, ASTM STP 939, American Society for Testing and Materials, Philadelphia, PA, 1987, pp. 224–240.
[54] J.F.R. Ambler, Effect of direction of approach to temperature on the delayed hydrogen cracking behavior of cold-worked Zr–2.5Nb, in: D.G. Franklin, R.B. Adamson (Eds.), Zirconium in the Nuclear Industry – Sixth International Symposium, ASTM STP 824, American Society for Testing and Materials, Philadelphia, PA, 1984, pp. 653–674.
[55] G.K. Shek, Ontario Hydro Technology Report A-NFC-95-102-P, 1995.
[56] J.F.R. Ambler, C.E. Coleman, Acoustic emission during delayed hydrogen cracking in Zr–2.5 wt% Nb alloy, in: Proceedings of Second International Congress on Hydrogen in Metals, Pergamon Press, Oxford, 1978 (Paper 3C10).
[57] C.E. Coleman, B.A. Cheadle, J.F.R. Ambler, P.C. Lichtenberger, R.L. Eadie, Can. Metall. Quart. 24 (1985) 245–250.
[58] C.E. Coleman, S. Sagat, G.K. Shek, D.B. Graham, M.A. Durand, Int. J. Pres. Ves. Pip. 43 (1990) 187–204.
[59] J. Crank, The Mathematics of Diffusion, 2nd ed., Clarendon Press, 1975. 69.
[60] D. Khatamian, J. Alloys Cmpds. 356–357 (2003) 22–26.
[61] D.A. Scarth, T. Smith, J. Pres. Ves. Tech. 123 (2001) 41–48.
[62] K. Nuttall, A.J. Rogowski, J. Nucl. Mater. 80 (1979) 279–290.
[63] M. Resta Levi, M.P. Puls, DHC Behaviour of Irradiated Zr–2.5Nb Pressure Tubes up to 365 °C, 18th International Conference on Structural Mechanics in Reactor Technology, 2005 (SMiRT 18, Paper G10-3).

[64] S. Sagat, M.P. Puls, Temperature Limit for Delayed Hydride Cracking in Zr–2.5Nb Alloys, 17th International Conference on Structural Mechanics in Reactor Technology, 2003 (SMiRT 17, Paper G06-4).
[65] C. Coleman, V. Grigoriev, V. Inozemtsev, V. Markelov, M. Roth, V. Makarevicius, Y.S. Kim, Kanwar Liagat Ali, J.K. Chakravartty, R. Mizrahi, R. Lalgudi, Nucl. Eng. Tech. 41 (2) (2009) 171–178.
[66] D.T. Peterson, H.M. Herro, Metall. Trans. 14A (1983) 17–21.
[67] S.M. Toy, J. Mater. Sci. 34 (1999) 181–189.
[68] L.S. Darken, Trans. Am. Inst. Min. Metall. Eng. 180 (1949) 430–438.
[69] G.K. Shek, M.T. Jovanovic, H. Seahra, Y. Ma, D. Li, R.L. Eadie, J. Nucl. Mater. 231 (1996) 221–230.
[70] Y.S. Kim, S.J. Kim, K.S. Im, J. Nucl. Mater. 335 (2004) 387–396.
[71] Y.S. Kim, S.B. Ahn and K.S. Kim, A model for delayed hydride cracking of zirconium alloys, in: 18th International Conference on Structural Mechanics in Reactor Technology, Beijing, 2005 (SMiRT 18, Paper C-07-2 633-641).
[72] Y.S. Kim, K.S. Kim, Y.M. Cheong, J. Nucl. Sci. Technol. 43 (2006) 1120–1127.
[73] Y.S. Kim, Mat. Sci. Eng. A 468–470 (2007) 281–287.
[74] Y.S. Kim, J. Nucl. Mater. 378 (2008) 30–34.
[75] Y.S. Kim, Y.M. Cheong, J. Nucl. Mater. 373 (2008) 179–185.
[76] Y.S. Kim, S.S. Park, J. Alloys Compds. 453 (2008) 210–214.
[77] Y.S. Kim, Mat. Sci. Eng. A 490 (2008) 146–150.
[78] M.P. Puls, J. Nucl. mater. 393 (2009) 350–367.